Probing the fusion of neutron-rich nuclei with re-accelerated radioactive beams

J. Vadas, Varinderjit Singh, B. B. Wiggins, J. Huston, S. Hudan, R. T. deSouza, Z. Lin, C. J. Horowitz, A. Chbihi, D. Ackermann, M. Famiano, and K. W. Brown

Phys. Rev. C **97**, 031601 — Published 27 March 2018

DOI: 10.1103/PhysRevC.97.031601

Probing the fusion of neutron-rich nuclei with re-accelerated radioactive beams

J. Vadas, Varinderjit Singh, B. B. Wiggins, J. Huston, S. Hudan, and R. T. deSouza*
Department of Chemistry and Center for Exploration of Energy and Matter, Indiana University 2401 Milo B. Sampson Lane, Bloomington, Indiana 47408, USA

Z. Lin and C. J. Horowitz
Department of Physics and Center for Exploration of Energy and Matter, Indiana University 2401 Milo B. Sampson Lane, Bloomington, Indiana 47408, USA

A. Chbihi and D. Ackermann
GANIL, 1 Blvd. Henri Becquerel, Caen, 14000, France

M. Famiano
Department of Physics, Western Michigan University, Kalamazoo, Michigan 49008, USA

K. W. Brown
National Superconducting Cyclotron Laboratory and Department of Physics and Astronomy, Michigan State University, East Lansing, Michigan 48824, USA
(Dated: February 1, 2018)

We report the first measurement of the fusion excitation functions for ^{39,47}K + ^{28}Si at near-barrier energies. Evaporation residues resulting from the fusion process were identified by direct measurement of their energy and time-of-flight with high geometric efficiency. At the lowest incident energy, the cross-section measured for the neutron-rich ^{47}K induced reaction is ∼6 times larger than that of the β-stable system. This experimental approach, both in measurement and analysis, demonstrates how to efficiently measure fusion with low-intensity, re-accelerated radioactive beams, establishing the framework for future studies.

PACS numbers: 21.60.Jz, 26.60.Gj, 25.60.Pj, 25.70.Jj

The recent coincident detection of gravitational waves in GW170817 [1] and a gamma ray burst in GRB170817A [2] marks the first observation of a binary neutron star merger [3, 4]. The delayed optical emission spectrum that followed indicated the presence of heavy elements in the neutron star ejecta [5]. This result clearly established binary neutron star mergers as an important, potentially primary, site for heavy element nucleosynthesis. Ejecta resulting from the tidal disruption of the neutron stars as they merge reflects both their initial composition as well as reactions that occur during the merger. Understanding the composition of the neutron stars is thus an important question in understanding heavy element nucleosynthesis.

Insight into the composition of some neutron stars prior to merging may be realized by considering the case of accreting neutron stars [6]. Heavy elements in the outer crust of an accreting neutron star are produced by fusion reactions [7, 8]. Some of the resulting heavy nuclei become neutron-rich through electron capture reactions [9]. It has been proposed that fusion of neutron-rich nuclei occurring in the outer crust may be enhanced relative to their β-stable counterparts providing an important heat source that triggers an X-ray superburst [10].

As a nucleus becomes increasingly neutron-rich, the extent of the neutron density distribution increases. Consequently, even if the density distributions were frozen through the fusion process the fusion cross-section would increase in response to the larger geometric cross-section. However, the fusion process is not static but dynamic. The decreased average binding energy of the outermost neutrons with increasing neutron number and the existence of low-energy collective modes act to make neutron-rich nuclei more polarizable. This increased polarizability, which can be viewed as the prelude to neutron transfer, increases the likelihood for fusion to occur. Thus, both static and dynamic factors impact the fusion cross-section. By examining the fusion cross-section with increasing neutron number for an isotopic chain and observing an increase beyond the geometric expectation, one might extract the increased role of dynamics. Such general expectations are borne out by microscopic time-dependent Hartree-Fock (TDHF) calculations [11].

To determine how fusion evolves for increasingly neutron-rich nuclei in an isotopic chain, it is advantageous to measure fusion at near-barrier energies. It is in this near and sub-barrier regime that one is most sensitive to the shape of the barrier which reflects both structure and dynamics. A new generation of radioactive beam facilities [12–14] with the capability of high-quality re-accelerated beams provide, for the first time, the opportunity to systematically address this question. These facilities together with facilities on the horizon [15]

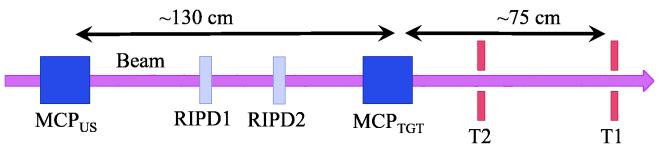

FIG. 1. (Color online) Schematic of the experimental setup. See text for details.

present the opportunity to examine fusion of neutron-rich nuclei approaching the neutron drip line. In this Rapid Communication we present the first measurement of the fusion excitation functions for ^{47}K + ^{28}Si and ^{39}K + ^{28}Si and establish the framework for future fusion studies.

This experiment was performed using the ReA3 facility at Michigan State University's National Superconducting Cyclotron Laboratory (NSCL). Ions of ^{39}K from a source or ^{47}K from a thermalized radioactive beam were charge bred in an ion trap, injected into the ReA3 80 MHz linac, and re-accelerated to energies between 2 and 3 MeV/A. The experimental setup used to measure fusion of potassium ions with silicon nuclei is depicted in Fig. 1. The beam first passed through an upstream E×B microchannel plate (MCP) detector, designated MCP$_{US}$, followed by another MCP detector in the target position (MCP$_{TGT}$) approximately 1.3 m downstream of the MCP$_{US}$. These detectors [16] provided a time-of-flight (TOF) measurement of the beam particles. The 327 μg/cm^2 thick ^{28}Si secondary emission foil of the MCP$_{TGT}$ served as the target for the experiment. This time-of-flight measurement allowed rejection of beam particles scattered or degraded prior to the target and provided a direct measure of the number of beam particles incident on the target. The intensity of the ^{39}K beam on the target was 3 - 4.5 × 10^4 ions/s, and that of the ^{47}K beam was 1 - 2.5 × 10^4 ions/s.

In order to identify contaminants in the ^{47}K beam, two compact axial field ionization chambers [17] designated RIPD1 and RIPD2 were inserted in the beam path between the two MCP detectors. Particle identification was achieved by ΔE-TOF, where the time-of-flight for each particle was measured between the MCP detectors. The energy distribution of incident ^{39}K and ^{47}K ions was measured by periodically inserting a silicon surface barrier detector just upstream of the target. The width, σ, of the energy distribution was ∼300 keV for ^{39}K and ∼600 keV for ^{47}K.

Fusion of a ^{39}K (or ^{47}K) projectile nucleus with a ^{28}Si target nucleus produces an excited ^{67}As (^{75}As) compound nucleus (CN). Near the fusion barrier, the excitation energy of the CN is ∼40 MeV (∼55 MeV). De-excitation of the CN via evaporation of light particles imparts transverse momentum to the evaporation residue (ER), allowing its detection in the annular silicon detectors designated T1 and T2 which subtend the angles 1.0° $\leq \theta_{lab} \leq$ 7.3°. This experimental approach provides an efficient means of measuring the fusion cross-section with beam intensities as low as 10^3 ions/s. While active target approaches have been successfully utilized to measure the fusion cross-section with low-intensity beams [18], with the present approach beam intensities as high as 10^6 ions/s can also be used providing efficient measurement with beams closer to β-stability. This technique has been used with stable beams [19] to measure cross-sections at the sub-millibarn level corresponding to sub-barrier energies [20].

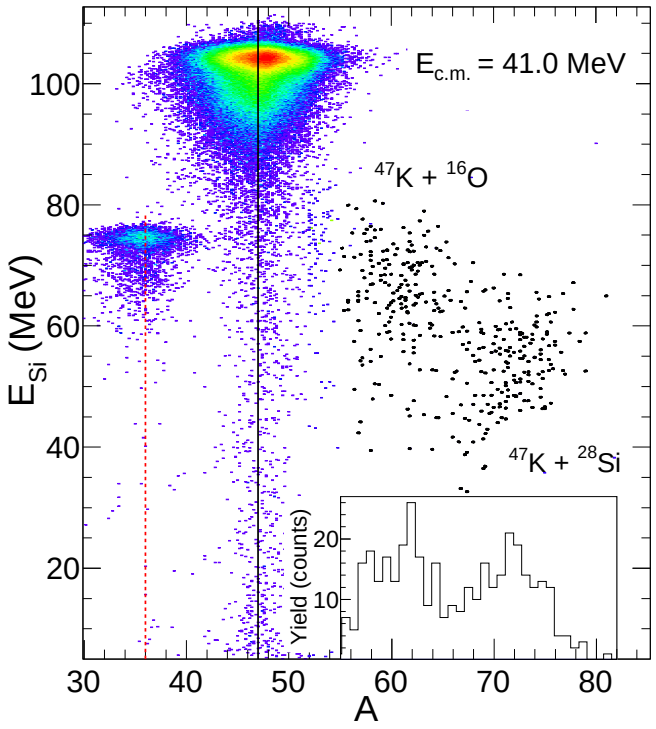

FIG. 2. (Color online) Energy versus mass number for reaction products with 2.4° $\leq \theta_{lab} \leq$ 7.3°. For reference, a solid (black) line and dashed (red) line are shown at A=47 and A=36, respectively. Evaporation residues are shown in bold. Inset: Mass distribution of evaporation residues.

To distinguish ERs from scattered beam, reaction products detected in the silicon detectors are identified by their mass using the energy vs. time-of-flight (E-TOF) technique [16, 19, 21], with the time-of-flight measured between the MCP$_{TGT}$ and the silicon detectors [22]. This mass identification for the ^{47}K beam is presented in Fig. 2. The intense peak evident at E$_{Si}$=105 MeV and A≈47 corresponds to elastically scattered ^{47}K particles, with the points extending down in energy along the solid A=47 line corresponding to scattered ^{47}K particles. Elastically scattered ^{36}Ar, a beam contaminant, is evident at E$_{Si}$=75 MeV centered on A=36, and accounts for <1% of the incident beam particles. Two distinct islands cleanly separated from the scattered beam particles are apparent at high mass (shown in bold). The inset

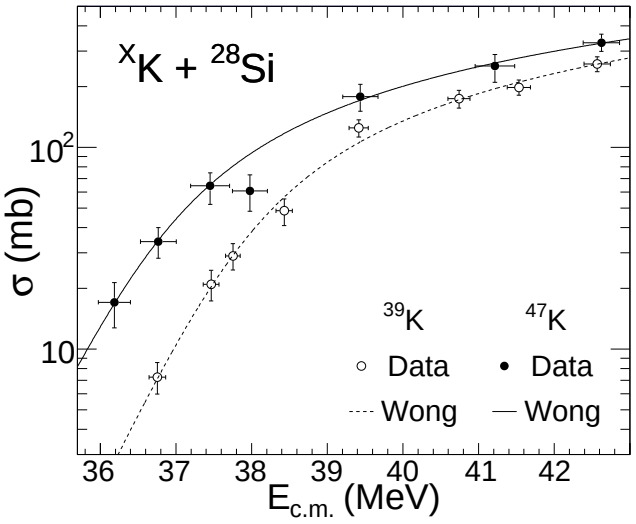

FIG. 3. Experimental fusion excitation functions for ^{39,47}K + ^{28}Si. Open and closed symbols depict the results for the ^{39}K and ^{47}K beams respectively. Dashed and solid lines correspond to a fit of the experimental data with the Wong parameterization.

shows the mass distribution of these islands, where a clear separation between the two islands is observed at A≈66. The lower mass island around A=60 corresponds to evaporation residues of compound nuclei formed following fusion of ^{47}K projectile nuclei with ^{16}O nuclei present in an oxide layer on the target foil (A_{CN}=63). The higher mass island peaking at A≈72 is populated by ERs following fusion of ^{47}K + ^{28}Si, which is consistent with the prediction of a fusion-evaporation code, EVAPOR [23]. ERs from the ^{28}Si target were selected using the two-dimensional E_{Si} *vs* A spectrum.

The measured yield of evaporation residues (N_{ER}) was used to calculate the fusion cross-section σ_{fusion} using σ_{fusion} = N_{ER} / (ϵ_{ER} × N_{Beam} × t), where ϵ_{ER} is the detection efficiency, N_{Beam} is the number of beam particles incident on the target and t is the target thickness. N_{Beam} was determined using the time-of-flight between the MCP detectors and particle identification in the ΔE-TOF spectrum. The thickness of the target was gauged using α particles from sources [24]. After accounting for the oxide layer, the ^{28}Si thickness was determined. The detection efficiency ϵ_{ER} was calculated by using EVAPOR [23] and the geometric acceptance of the silicon detectors. For both systems, the combined geometric efficiency of T1 and T2, for all incident energies measured, was ∼80%.

The fusion cross-sections as a function of incident energy for ^{39}K + ^{28}Si (open circles) and ^{47}K + ^{28}Si (closed circles) are shown in Fig. 3. The uncertainty in $E_{c.m.}$ reflects the spread in the beam energy measured just upstream of the target, while the uncertainty in the fusion cross-sections includes both measurement statistics and systematic errors. Both fusion excitation functions exhibit the general trend expected for a barrier-driven process. With decreasing incident energy, the fusion cross-section decreases slowly for energies above the barrier then drops dramatically at and below the barrier. To facilitate comparison of the two systems, the measured fusion excitation functions were parameterized using a functional form that describes the penetration of an inverted parabolic barrier (Wong formula) [25]. The fits of the ^{39}K and ^{47}K data are shown in Fig. 3 as the dashed and solid lines respectively. With the exception of the ^{47}K cross-section measured at $E_{c.m.}$∼38 MeV the excitation functions for both systems are reasonably well described by this parameterization.

In order to better understand the extent to which the observed fusion cross-sections are due to the nuclear size, structure, or dynamics, we have calculated the fusion of potassium isotopes with ^{28}Si nuclei with different models. The simplest model utilized is a Sao Paulo (SP) model [26], which allows one to assess the changes in the fusion cross-section due solely to the changes in the density distributions of the nuclei. These density distributions have been calculated within a relativistic mean field (RMF) model [27, 28], and were utilized in a folding potential to predict the fusion cross-sections. As the density distributions are spherically symmetric, initial deformation of the projectile and target nuclei are ignored in this approach. The cross-section predicted from the RMF+SP model is depicted in Fig. 4 as the dash-dot (green) line. While this static model provides reasonable agreement at above-barrier energies, it significantly underpredicts the measured cross-sections at energies near and below the barrier for both reactions, indicating that the size of the colliding nuclei alone is insufficient to explain the observed fusion cross-sections.

TABLE I. Woods-Saxon potential parameters for the measured systems.

	V_0 (MeV)	r_0 (fm)	a (fm)
^{39}K + ^{28}Si	-55.03	1.16	0.612
^{47}K + ^{28}Si	-55.97	1.16	0.622

For mid-mass stable nuclei, the role of dynamics (collective modes) in describing the fusion cross-section in the near-barrier regime is well established [29]. We elected to explore the role of dynamics using coupled channels calculations [30] which have been successful at describing the fusion of stable and near β-stable nuclei [29].

The coupled channels calculations performed to describe the fusion of potassium and silicon nuclei utilized the code CCFULL [31], with the potential parameters shown in Table I. For these calculations, coupling to the 1/2+ ground state and the 3/2+ and 5/2+ excited states of ^{47}K were included, and considered to be members of a rotational band. For ^{39}K, the 3/2+ ground state and

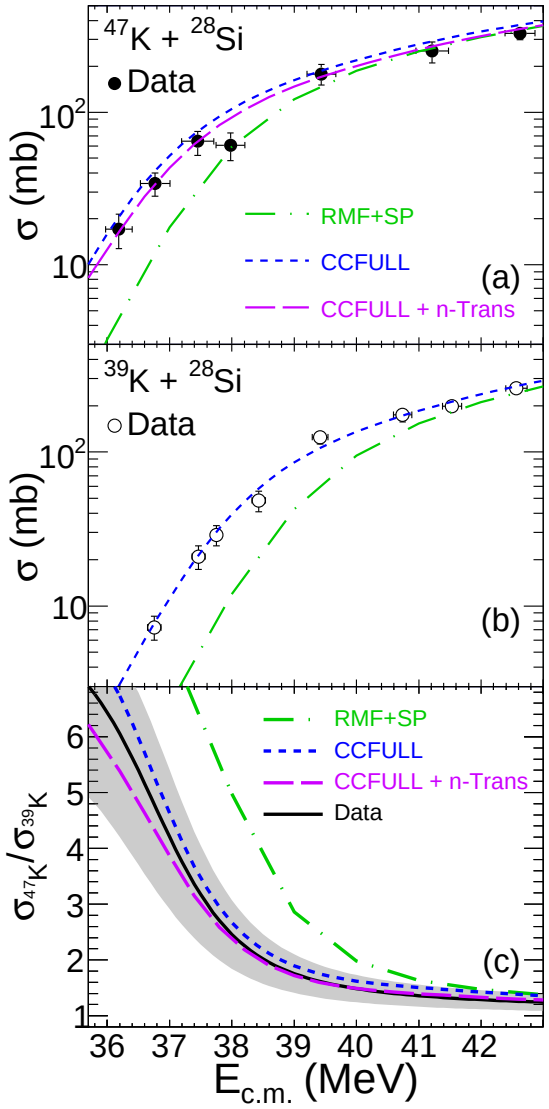

FIG. 4. (Color online) Panel (a): Experimental data for ^{47}K + ^{28}Si are represented by symbols. Dashed (colored) lines correspond to different models described in the text. Panel (b): Same as above for ^{39}K projectile ions. Panel (c): The relative cross-section, $\sigma(^{47}\mathrm{K})/\sigma(^{39}\mathrm{K})$ is depicted as a solid (black) line, corresponding to the ratio of the Wong fits of the experimental data. The shaded band represents the measurement uncertainty. The dashed (colored) lines correspond to model calculations described in the text.

excited 5/2+ and 7/2+ levels were included. Coupling in the ^{28}Si target nucleus included the 2+ and 4+ levels of the rotational band built on the 0+ ground state. The results of these calculations are shown in Fig. 4 as the short-dashed (blue) line. While in the case of ^{39}K + ^{28}Si (panel b) the CCFULL calculations provide a good description of the experimental cross-sections, for the ^{47}K induced reaction (panel a) the model slightly overpredicts the data. Although neutron transfer plays no role in the case of ^{39}K due to the associated negative Q-value, in the case of ^{47}K, Q_{2n} = 3.844 MeV, suggesting that neutron transfer may play a role. We therefore included neutron transfer channels in the CCFULL calculations of the ^{47}K induced reaction. The strength of the coupling for neutron transfer, F_t has a value ranging between zero and unity [31]. Inclusion of a coupling with F_t = 0.25 provides the best description of the experimental data, as shown by the dashed (purple) line in Fig. 4(a). Increasing the coupling strength for neutron transfer above F_t = 0.35 significantly underpredicts the measured cross-sections in the energy range shown. The reduction in the fusion cross-section with the inclusion of neutron transfer above the barrier is likely associated with transfer that does not lead to fusion. At energies below the barrier, outside the presented energy regime, inclusion of neutron transfer results in an enhancement in the fusion cross-section as expected.

In addition to examining the fusion excitation functions, it is also instructive to construct the relative cross-section, $\sigma(^{47}\mathrm{K})/\sigma(^{39}\mathrm{K})$, as presented in Fig. 4(c). For an isotopic chain, examining the relative cross-section is valuable as it removes the average behavior of the Coulomb-dominated, barrier-driven process emphasizing the change in the nuclear potential with increasing neutron number. This ratio also results in cancellation of systematic errors common to the measurement of both excitation functions. For energies above the barrier, the ratio for the experimental data is essentially flat with a value of ∼1.2, but as $E_{c.m.}$ decreases to and below the barrier, the ratio rapidly increases to a factor of ∼6 at the lowest measured energy.

All the model calculations shown in Fig. 4(c) exhibit the same qualitative trend exhibited by the data. At the highest energies measured, all of the model calculations converge and are in good agreement with the experimental data. This result is unsurprising, as the cross-section at above-barrier energies are dictated by the geometric cross-section. For energies below the barrier, all the models shown exhibit the trend of increasing relative cross-section with decreasing $E_{c.m.}$. The increase in the relative cross-section with decreasing energy reflects both the larger size of the neutron-rich nucleus, specifically the increased extent of its neutron density distribution, and the dynamics associated with the additional neutrons. The RMF+SP model, with static density distributions, manifests the onset of this rapid increase in the relative cross-section energy at a higher energy than the data. As expected from their agreement with the excitation functions, the CCFULL calculations both excluding and including neutron transfer provide a reasonably good description of the measured relative cross-section within the measurement uncertainties (shaded region). These uncertainties are dominated by the statistical quality of the data. Improvements made after the experiment will enable future experiments to acquire data of better statistical quality.

In this work we present a new, efficient approach to the measurement of fusion excitation functions with low-intensity re-accelerated radioactive beams. By utilizing isotopic chains and constructing the relative fusion cross-section, the impact of the additional neutrons on fusion is assessed. This new approach is well matched to the new generation of radioactive beam facilities, both in existence and on the horizon, and will allow extraction of the dependence of fusion on neutron number for the most neutron-rich nuclei where detailed structure information is unavailable.

We thank the staff at NSCL, Michigan State University, and in particular those at the ReA3 facility for providing the high quality beams that made this experiment possible. The high quality ^{28}Si targets, provided by M. Loriggiola, Legnaro National Laboratory, are deeply appreciated. This work was supported by the U.S. Department of Energy under Grant Nos. DE-FG02-88ER-40404 (Indiana University), DE-FG02-87ER-40365 (Indiana University Nuclear Theory), DE-SC0008808 (NUCLEI SciDAC Collaboration), DE-NA0002923 (Michigan State University), and the National Science Foundation under Grant Nos. PHY-1565546 (Michigan State University) and PHY-1712832 (Western Michigan University). J.V. acknowledges the support of a NSF Graduate Research Fellowship under Grant No. 1342962. One of us (D.A.) is supported by the European Commission in the framework of the CEA-EUROTALENT program.

* desouza@indiana.edu

[1] LIGO Scientific Collaboration and Virgo Collaboration, GCN , 21505 (2017).
[2] A. Goldstein *et al.*, Astro. Phys. Jour. Lett. **848**, L14 (2017).
[3] LIGO Scientific Collaboration and Virgo Collaboration, Astro. Phys. Jour. Lett. **848**, L13 (2017).
[4] LIGO Scientific Collaboration and Virgo Collaboration, Phys. Rev. Lett. **119**, 161101 (2017).
[5] M. Nicholl *et al.*, Astro. Phys. Jour. Lett. **848**, L18 (2017).
[6] T. Strohmayer and L. Bildsten, *Compact Stellar X-ray Sources* (Cambridge University, 2006) p. 113.
[7] H. Schatz *et al.*, Phys. Rev. Lett **86**, 3471 (2001).
[8] S. E. Woosley *et al.*, Astrophys. J. Suppl. **151**, 75 (2004).
[9] S. Gupta *et al.*, Astrophys. J. **662**, 1188 (2007).
[10] C. J. Horowitz, H. Dussan, and D. K. Berry, Phys. Rev. C **77**, 045807 (2008).
[11] A. S. Umar, V. E. Oberacker, and C. J. Horowitz, Phys. Rev. C **85**, 055801 (2012).
[12] M. J. G. Borge, Acta Phys. Pol. B **47**, 591 (2016).
[13] S. Gales, J. Phys.: Conf. Ser. **267**, 012009 (2011).
[14] O. Kester *et al.*, Proceedings, 25th International Linear Accelerator Conference, LINAC2010: Tsukuba, Japan, September 12-17, 2010 , MO203 (2011).
[15] G. Bollen, AIP Conf. Proc. **1224**, 432 (2010).
[16] T. K. Steinbach *et al.*, Nucl. Instr. and Meth. **A743**, 5 (2014).
[17] J. Vadas *et al.*, Nucl. Instr. and Meth. **A837**, 28 (2016).
[18] P. F. F. Carnelli *et al.*, Phys. Rev. Lett. **112**, 192701 (2014).
[19] T. K. Steinbach *et al.*, Phys. Rev. C **90**, 041603(R) (2014).
[20] T. K. Steinbach, Ph.D. thesis, Indiana University (2016).
[21] V. Singh *et al.*, Phys. Lett. B **765**, 99 (2017).
[22] R. T. deSouza *et al.*, Nucl. Instr. and Meth. **A632**, 133 (2011).
[23] N. G. Nicolis and J. R. Beene, unpublished (1993).
[24] J. F. Ziegler, M. D.Ziegler, and J. P. Biersack, Nucl. Instr. and Meth. **B268**, 1818 (2010).
[25] C. Y. Wong, Phys. Rev. Lett. **31**, 766 (1973).
[26] L. R. Gasques *et al.*, Phys. Rev. C **69**, 034603 (2004).
[27] P. Ring, Prog. Part. Nucl. Phys. **37**, 193 (1996).
[28] B. D. Serot and J. D. Walecka, Adv. Nucl. Phys. **16**, 1 (1986).
[29] G. Montagnoli *et al.*, Phys. Rev. C **87**, 014611 (2013).
[30] C. H. Dasso, S. Landowne, and A. Winther, Nucl. Phys. A **405**, 381 (1983).
[31] K. Hagino, N. Rowley, and A. T. Kruppa, Comput. Phys. Commun. **123**, 143 (1999).